processes

MDPI

Article

Random Forest-Based Wire Cut Electro-Discharge Machining of Physella Acuta Shell Particles Reinforced AA1050 Composite with Microstructural Analysis

Rajesh Jesudoss Hynes Navasingh [1,*], D. S. Samuvel Prem Kumar [1], Senthil Kumar Jagatheesaperumal [2] and Angela Jennifa Sujana Jesudoss [3]

[1] Department of Mechanical Engineering, Mepco Schlenk Engineering College, Sivakasi 626005, Tamil Nadu, India; prem194731@gmail.com
[2] Department of Electronics and Communication Engineering, Mepco Schlenk Engineering College, Sivakasi 626005, Tamil Nadu, India; senthilkumarj@mepcoeng.ac.in
[3] Department of Artificial Intelligence & Data Science, Mepco Schlenk Engineering College, Sivakasi 626005, Tamil Nadu, India; ang_jenefa@mepcoeng.ac.in
* Correspondence: findhynes@yahoo.co.in

Abstract

The high strength and light weight of aluminum matrix composites have made them the material of choice for many engineering applications. Snail shells and other bio-reinforcements offer a potential substitute for conventional ceramic reinforcements. However, the inherent difficulty in machining Aluminum Matrix Composites (AMCs) stems from the presence of reinforcing particles. This study investigates the machinability of aluminum matrix composites (AMCs) reinforced with Physella Acuta snail shell (PAS) particles using Wire Electrical Discharge Machining (WEDM) with a zinc-coated brass wire electrode. The primary objective is to determine how various input elements affect process conditions to achieve the desired surface quality. In order to do this, the Random Decision Forest approach was employed. Scanning Electron Microscopy (SEM) evaluation revealed the presence of microvoids, surface defects, deep craters, and crack propagation. It was found that the random forest method had an F1-score of 0.94, a recall of 0.96, and a precision of 0.97. The optimized parameters yielded an MRR of 0.5 mm^3/min, SR of 2.14 µm, and EWR of 0.017.

Keywords: aluminum matrix composite; snail shell reinforcement; zinc coated brass wire; decision tree; Material Removal Rate (MRR); Electrode Wear Rate (EWR)

check for updates

Academic Editor: Chin-Hyung Lee

Received: 24 June 2025
Revised: 5 August 2025
Accepted: 6 November 2025
Published: 8 November 2025

Citation: Navasingh, R.J.H.; Kumar, D.S.S.P.; Jagatheesaperumal, S.K.; Jesudoss, A.J.S. Random Forest-Based Wire Cut Electro-Discharge Machining of Physella Acuta Shell Particles Reinforced AA1050 Composite with Microstructural Analysis. *Processes* **2025**, *13*, 3621. https://doi.org/10.3390/pr13113621

Copyright: © 2025 by the authors. Licensee MDPI, Basel, Switzerland. This article is an open access article distributed under the terms and conditions of the Creative Commons Attribution (CC BY) license (https://creativecommons.org/licenses/by/4.0/).

1. Introduction

The field of contemporary engineering is characterized by an unwavering search for novel materials and machining methods. Among them, bio-ceramic reinforced composites have become a viable option due to their favorable combination of corrosion resistance, mechanical strength, and biocompatibility, properties essential for a wide range of applications, from biomedical implants to aerospace [1]. In this context, WEDM has attracted a lot of attention due to its precision and adaptability while machining complex shapes [2] and machining of aluminum metal matrix composites [3]. Silicon carbide is incorporated into the aluminum alloy to strengthen it and improve its mechanical properties [4]. However, adding 5 weight percent silicon carbide to AA 1050 enhances hardness, which complicates the machining process and reduces tool life and MRR [5,6]. Boron carbide reinforced AMC

has good mechanical qualities, but because of its hardness, built-up edge, and abrasiveness, it is challenging to machine using conventional machining techniques [7]. Since there is no direct contact between the specimen and the tool, WEDM is the suggested technique, as noted by Farooq et al. [8]. WEDM uses dielectric fluid as a medium and sparks produced by electrical energy between the specimen and the tool to maintain a distance between them [9]. Molds, dies, irregularly shaped components, and curved shapes can be produced with excellent precision and surface polish using the WEDM method [10]. In order to understand the influence of electrical input parameters on material removal rate (MRR), surface roughness (SR), and electrode wear rate (EWR), many studies were carried out. In order to optimize solutions for the process, a parametric analysis of dry wire cut machining on cemented tungsten carbide was conducted by Shayan et al. [11]. Chaubey investigated the surface quality of helical and bevel gears manufactured using WEDM, concentrating on material processing. [12]. Using a tungsten–thorium electrode, Mandaloi [13] examined the effects of process parameters on MRR, EWR, and SR on AISI M2 steel. Kumar et al. (2018) used a modeling and multi-response optimization of WEDM parameters for machining of aluminum metal matrix composite [14]. With an emphasis on attaining high precision, Ishfaq [15] optimized WEDM for accurate machining of a newly designed Al6061–7.5% SiC composite squeeze-cast specimen. Pramanik and Littlefair [16] examined the wire EDM machining of metal matrix composites with variations in reinforced particle size in order to gain a better knowledge of the machining process.

Gopal et al. used electro discharge machining in hybrid MMC made of magnesium, boron nitride, and carbon nanotubes (CNTs), and looked into how machining was affected by wire feed, concentration, and size of reinforced particle as well as discharge duration (Td) and pulse gap (Tg). They found that SR and the MRR are significantly influenced by Discharge Duration (Td) [17]. Suresh and Sudhakara found that when the SiC reinforcement in Al 7075 MMC is increased, SR increases and MRR decreases [18]. It was reported that Al6351/SiC/B4C composites with a high boron carbide concentration have a broader kerf and poor surface quality [19]. In machining AA 6061-T6/15 weight percentage of SiC, Pandiyan et al. examined the role of parameters such as Pulse Gap, Discharge Current, and Discharge Duration. They discovered that greater MRR and SR are caused by an increase in Discharge Duration and Discharge Current [20]. After examining the impact of process variables, Lal et al. discovered the best outcomes when milling Al7075/SiC/Al_2O_3 composite [21]. Dey and Pandey examined how process parameters influence Al6061/Cenosphere composites during machining. They found that parameters like Discharge Duration (TD) and Pulse Gap (TG), and the concentration of reinforced particles influence cutting speed, SR, and Kerf Width [22]. In the Wire-EDM process, the electrode is a crucial factor, and researchers have used different kinds of electrodes based on the properties of the materials. Electrode wires, such as bare wire and thin-coated electrode wire, result in a high-quality machining process, as observed by Raza et al. [23]. Reolon et al. used brass and zinc-coated copper wire for their research to find the impact of wire type on the machining process of IN 718 alloy. They discovered that zinc-coated copper wire yields good results for Kerf Width, with the coated wire contributing to a 35% increase in wire feed rate [24]. Manjaiah et al. examined machining of TiNiCu alloy using zinc-coated brass wire, and observed faster machining rates and reduced outer surface roughness [25]. Research was carried out by Nourbakhsh et al. [26] to compare the performance of zinc-coated brass wire and high-speed brass wire in machining Ti 6Al 4V grade 5. Brass wire coated in zinc yielded better results, with increased cutting speed and a good surface finish [27]. When Shandilya et al. [28] compared Artificial Neural Networks (ANN) with Surface Response Methodology (RSM), they found that the ANN model provided more accurate output values. Rao and Krishna [29] studied the machining of SiC reinforced Al 7075, considering the output

parameters of SR, MRR, and Wire Wear Ratio using Surface Response Methodology. A hybrid gray fuzzy reasoning methodology was applied to study the wear behavior of Al-MMC reinforced with coconut shell ash [30]. Using the stir casting method and coconut fly ash reinforcement in weight percentages of 3, 6, and 9, Prakash et al. [31] developed AMC and studied their performance. Tribological, morphological, and corrosion tests were carried out on Al 98SN S2 with a 2 weight % of snail shell reinforcement by Pruncu et al. In comparison to SiC, they found that the addition of snail shell particles lowers wear and corrosion rates [32].

Although progress has been made in WEDM of aluminum matrix composites, little research has been conducted on the machining of sustainable bio-ceramic reinforcements. Previous studies predominantly utilize conventional statistical methods for process optimization, underscoring the need for the implementation of machine learning approaches for predictive modeling and performance improvement. This study fills these gaps by combining bio-ceramic reinforcements with machine learning-based optimization techniques to enhance machining efficiency, surface quality, and sustainability. The purpose of this work is to investigate how zinc-coated brass wire affects the surface roughness, rate of material removal, and electrode wear ratio during machining employing Taguchi and machine learning techniques.

2. Materials and Methods

Particulates of snail shell [32] are added as reinforcement (3% wt.), while pure aluminum is used as the matrix material. The composition of AA1050 is given in Table 1 [32], and the XRD pattern of the snail shell powder is shown in Figure 1.

Table 1. Chemical Composition of AA1050.

Material	Mn	Zn	Si	Fe	Mg	Cu	Ti	Ni	Pb	Al
Wt. %	0.03	0.07	0.30	0.40	0.03	0.03	0.03	0.03	0.03	Bal

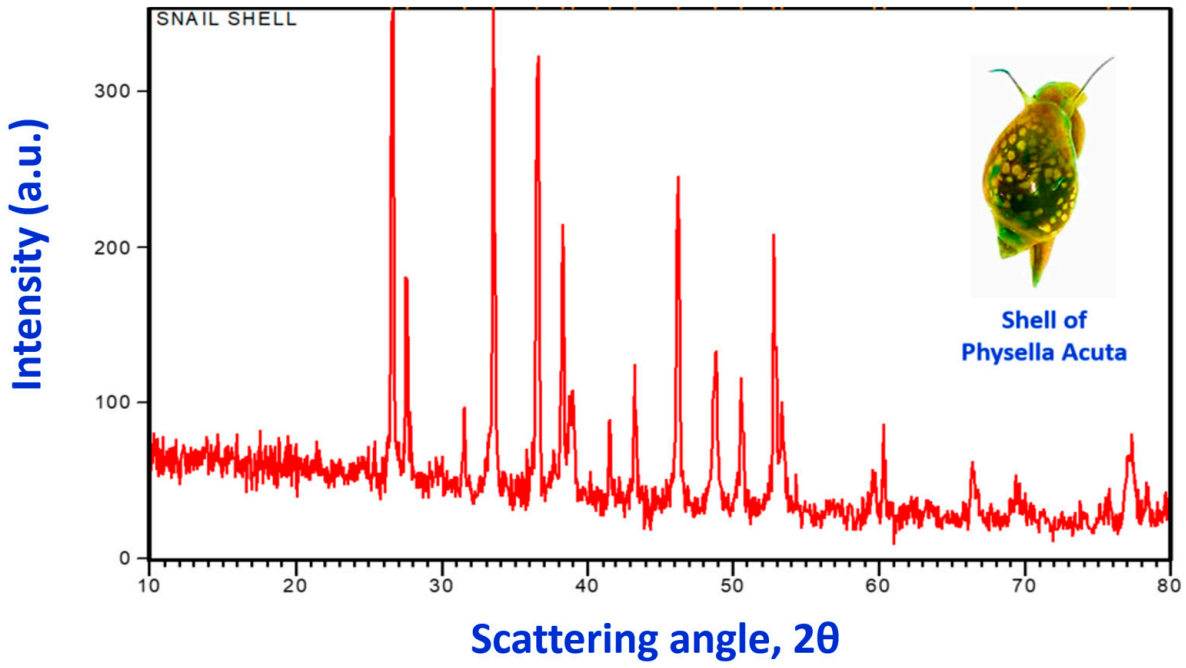


Figure 1. XRD of Physella Acuta Snail Shell powder.

Al-MMC is developed (Figure 2) by the Bottom Pour Stir Casting process and machined by WEDM (Table 2).

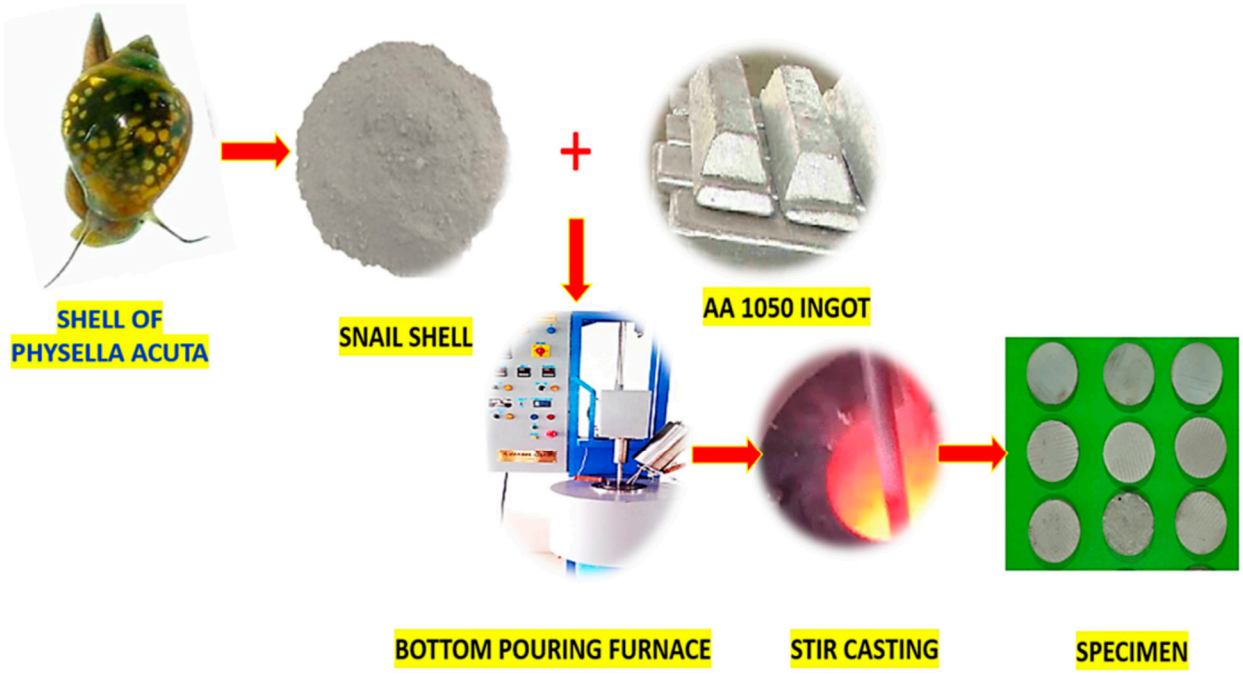


Figure 2. Preparation of snail shell reinforced AA1050 composite.

Table 2. Process conditions in stir casting.

S.No	Stirring Speed Rpm	Stirring Temperature °C	Reinforcement Preheat Temperature °C	Blade Angle
01.	300–600	630–650	500 in 30 min	45° and 60°

The bulk density of the Physella Acuta Shell (PAS) reinforcement is approximately 2.8 g/cm^3. The X-ray diffraction (XRD) pattern of the snail shell powder (Figure 1) reveals its crystalline nature and mineralogical composition, which are critical for its potential application as a reinforcement material in composite structures. The XRD spectrum spans a diffraction angle (2θ) range from approximately 10° to 80°, with multiple sharp and intense peaks observed predominantly between 20° and 60°, indicating a highly crystalline structure. The most prominent diffraction peaks correspond to $CaCO_3$, which is the primary constituent of snail shells, occurring predominantly in its aragonite and calcite phases. The presence of these well-defined peaks confirms the dominance of crystalline $CaCO_3$, with aragonite being the thermodynamically favored phase in biogenic materials such as shellfish shells. The high intensity of specific peaks further suggests a significant degree of crystallinity, which is desirable for reinforcement applications as it contributes to mechanical stability and structural integrity. Additionally, a minor amorphous background in the spectrum, indicated by slight elevations in the baseline intensity, suggests the presence of organic components or residual impurities within the snail shell powder. The identification of these crystalline phases is essential for assessing the suitability of snail shell powder as a reinforcement material in aluminum matrix composites, where the inherent properties of $CaCO_3$, such as hardness and thermal stability, can enhance the mechanical characteristics of the composite. The diffraction data further validate that the material has undergone appropriate calcination and grinding processes, ensuring optimal phase retention for structural reinforcement applications. These findings suggest that snail shell powder can serve as a viable, eco-friendly alternative to synthetic ceramic reinforcements,

offering potential benefits in lightweight engineering materials, bioceramics, and wear-resistant coatings.

Snails are collected, then washed and finally ground into fine powder. The average PAS particle size ranges from 30 to 45 µm (after grinding and sieving), and the melting point of PAS is around 825 °C. The metal matrix (AA 1050 aluminum ingots) has high corrosion resistance, excellent thermal conductivity, and ductility. 3% from the total weight (of the snail-shell powder) is added to the molten, when the aluminum itself is molten, and stirred for homogeneous distribution. The aluminum alloy and the snail shell powder are the melt, and they are fully fused with each other through the stir casting process, and the mechanical stirrer ensures the wetting of the reinforcement and aluminum matrix. The molten aluminum-snail shell composite is then cast into molds to cool and harden into the desired shapes (Figure 2). The specimens are depicted in Figure 3. A machine (Suzhou Tiantong Aike Intelligent Technology Co., Ltd., Suzhou, China) is utilized to execute the cutting operation using 0.25 mm diameter zinc-coated brass wire (Table 3). Distilled water, applied at a flushing pressure of one bar, served as the dielectric fluid. It is well-established that higher cutting speeds can increase MRR but often at the expense of surface finish, leading to more significant cratering and thermal damage [33]. Three essential input parameters—open voltage, Pulse ON time, Pulse OFF time—were selected for each experimental run during the study of machining performance (Table 4). After conducting trial runs, the ideal ranges for the starting values were identified. The surface roughness of the workpiece after machining is measured with a surface roughness tester (Model: sj-210, Mitutoyo, Kanagawa, Japan). For every workpiece, the average of three readings is taken into account. Based on previous studies [34,35], zinc-coated wire was used for the studies due to its improved performance in machining AMCs. Key variables, namely Open Voltage (VO), Total Discharge (TD), and Tool Gap (TG), were taken into consideration while using an L9 design for Taguchi-based experimentation.



Figure 3. Specimen cut for Wire-cut Electro Discharge Machining.

Table 3. Initial Setting parameters of WEDM.

S.No	Parameter	Setting Value
01.	Dielectric Fluid	Distilled Water
02.	Flushing Pressure [bar]	1
03.	Cutting Length	60 mm
04.	Wire tension [g]	2
05.	Wire diameter [mm]	0.25
06.	Wire Electrode Polarity	Negative
07.	Wire Speed [mm / min]	10
08.	Pulse OFF time (Average)	6.5 microseconds

Table 4. Selected ranges of input parameters.

Factors	Levels			Responses
	−	0	+	
Voltage (V)	60	70	80	Material Removal Rate
Pulse ON time (µs)	1	2	4	Surface Roughness
Current (Amps)	0.5	1	1.5	Electrode Wear Ratio

In this study, MRR and EWR are mathematically calculated as follows.

$$MRR = \frac{Wa - Wb}{Tmx\rho} \; EWR = \frac{Wa - Wb}{Wa} \times 100 \quad (1)$$

Wa—Specimen weight before machining
Wb—Specimen weight after machining
ρ—Density of the specimen
T_m—Machining time

3. Results and Discussion

3.1. Micro Structural Evaluation

The SEM image (Figure 4) shows the surface of the Al97SNS3 specimen. The aluminum matrix (AA1050) is shown by the dark smooth regions. The lighter, more asymmetrical shapes are most likely the reinforced snail shell particles in the matrix. Particles of snail shell vary in size and shape, but overall, the distribution appears to be uniform (Figure 4a). Achieving uniform mechanical characteristics across the composite depends on this homogeneity. It looks like there is a strong bond at the contact between the snail shell particles and the aluminum matrix (Figure 4b). Effective load transfer from the matrix to the reinforcement, which increases the overall strength of the composite, depends on good interfacial bonding. The SEM images are analyzed using specialized software (Mountains® 11.0, Digital Surf, Besançon, France) that allows for measuring the size of craters and voids, and the length of cracks. During the SEM evaluation, it was found that microvoids are in the range of 7 microns to 12 microns, and craters are in the range of 28 microns to 34 microns. Microcracks seem to begin as a result of thermal stresses. Micro and macro void formation mechanisms due to incomplete melting and thermal stress during casting and WEDM.

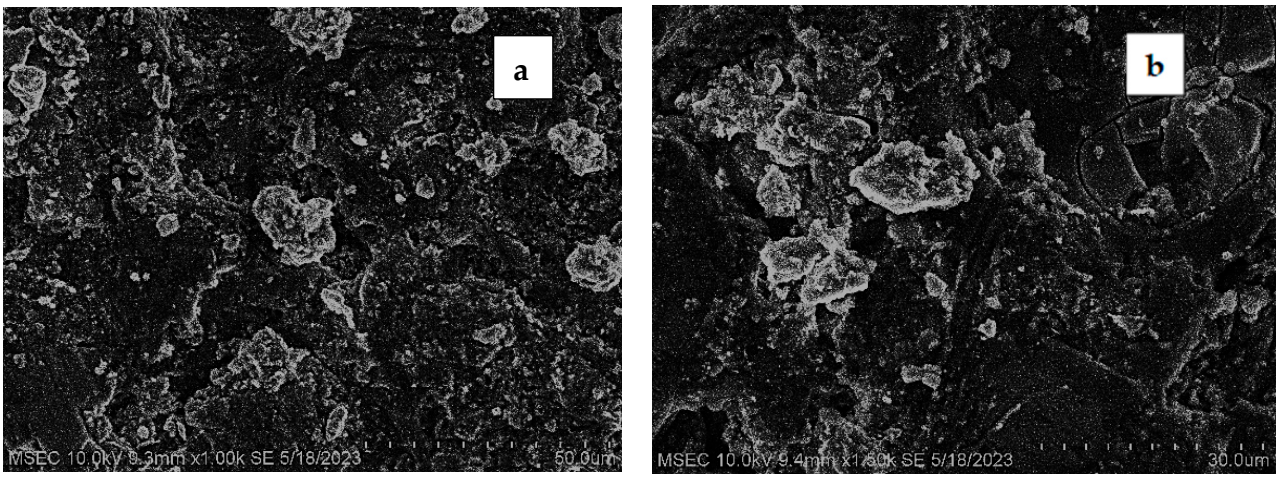


Figure 4. Microstructure of specimen before machining (**a**) Uniform distribution in aluminum matrix (**b**) Appearance of snail shell particles.

After machining the specimen, the presence of micro voids (Figure 5a) and pore holes (Figure 5b) are observed. It is noted that the presence of Snail Shell increases the surface roughness and decreases electrical conductivity. The Snail Shell particle did not fully melt at the specified temperature, so its full size is visible. This suggests the surrounding matrix is melted and vaporized, creating small craters and debris throughout the composite. The Snail Shell ceramics shielding decreases MRR and increases the roughness of the surface. The electric discharge during the machining is the primary factor that determines the crater's size on the workpiece.

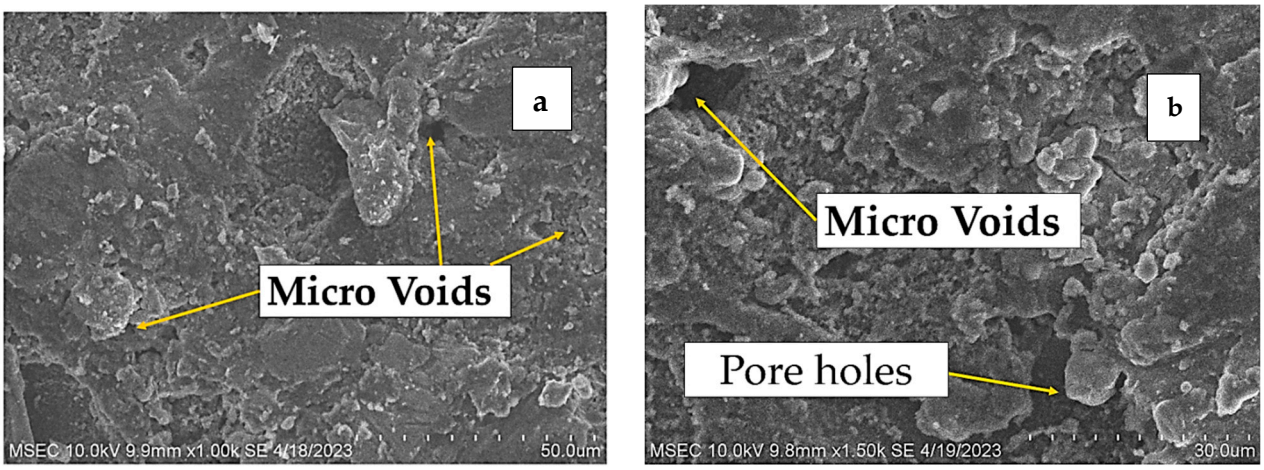
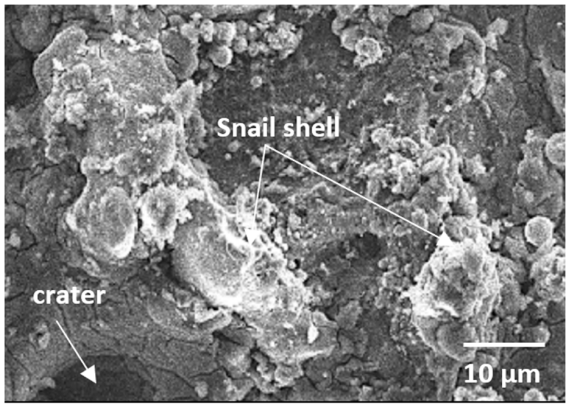


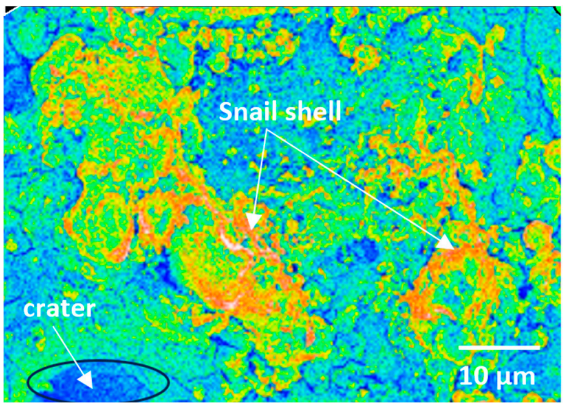
Figure 5. Microstructure of specimen after Machining. (**a**) Presence of micro voids (**b**) Micro voids and pore holes.

The detailed examination of the machined surface of Physella Acuta Shell (PAS) reinforced AA1050 composite is shown in Figure 6. Different image processing and image segmentation techniques were deployed to study the surface features, particle distribution, and material behavior in response to WEDM. SEM Micrograph (Figure 6a) shows the machined surface, exhibiting snail shell features and craters due to the high-temperature influence of WEDM. Craters are due to localized melting and material removal during WEDM. Colorized Micrograph (Figure 6b) improves the contrast between regions, thereby enhancing the differentiation of the PAS reinforcement, the aluminum matrix, and the heat-affected zones. Slice Analysis (Figure 6c) gives a quantitative intensity distribution

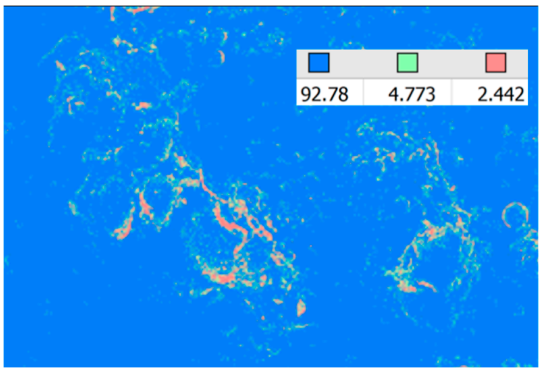
of surface features. The distribution and density of the particles were analyzed using a threshold detection approach.



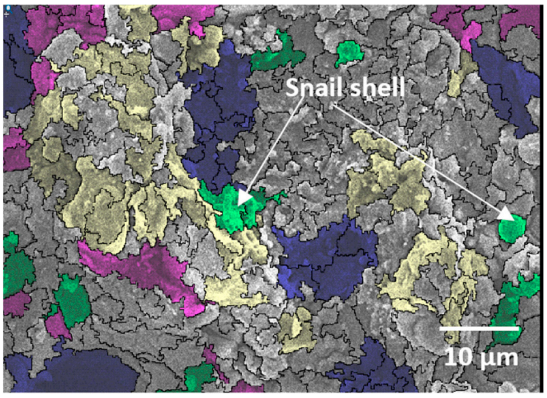
(**a**)



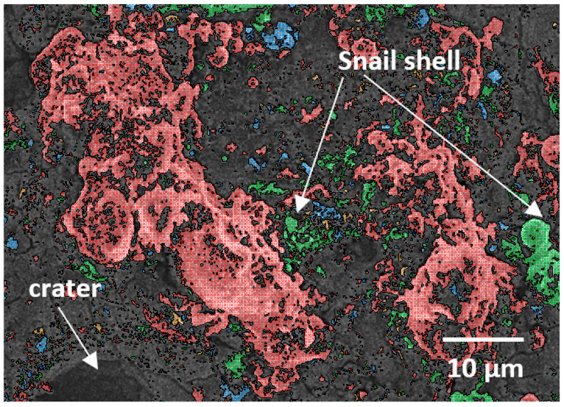
(**b**)



(**c**)



(**d**)



(**e**)

Information		
Method	Threshold detection	
Channel	WEDM 1 > Extracted area	
Number of particles	11,484	
Coverage	40.55	%
Density	2.829	Particles/mm²
Individual results		
Parameters	Area	
Unit	mm²	
Particle #1	0.03241	
Particle #2	0.02067	
Particle #3	0.7279	
Particle #4	0.02149	
Global statistics		
Mean	0.1438	

(**f**)

Figure 6. Microstructural Analysis (**a**) SEM Micrograph (**b**) Colorized Micrograph (**c**) Slice Analysis (**d**) Segmented Micrograph (**e**,**f**) Particle Analysis.

Segmented micrograph (Figure 6d) distinguishes the different phases present within the composite. The PAS reinforcement and aluminum matrix are distinguished from one another, enabling a more accurate assessment of particle distribution, agglomerations, and voids or defects created by WEDM. The particle area analysis (Figure 6e) and how particles of different sizes and characteristics map to this distribution (Figure 6f). Various groups of particles are recognized, and the contributions of each group to the total

composite area are quantified. Total number of particles analyzed. In this case, the total number of particles is 1944. The area values represent the size of individual particles in μm^2, helping to assess the distribution of particle sizes. Area Coverage shows the total area covered by the particles in the sample. This means that particles account for 42.35% of the analyzed area, indicating how much of the surface area is covered by the particles. These area values indicate the relative size of each particle, with Particle #2 being the largest (0.3217 μm^2) and Particle #3 the smallest (0.1937 μm^2). The size of the particles (as measured in μm^2) can have a direct impact on the roughness and MRR during material processing. When particles are larger, they might create larger surface indentations during machining, resulting in higher surface roughness. In contrast, smaller particles might lead to finer, smoother surfaces. Looking at the Area data in the table (such as Particle #1, Particle #2, and Particle #3), larger particles with higher surface area could cause larger material disturbances during processing, affecting both roughness and material removal rates. Mean particle area (0.148 mm^2) is significant to the extent of particle dispersion, which plays a significant role in a few mechanical properties after the machining, such as wear resistance and hardness. This is explained by the thermal action of the WEDM, which leads to the formation of a heat-affected zone, with this effect being favorable to the PAS-reinforced AA1050. The particle distribution assessment indicates a relatively consistent distribution of PAS into the aluminum matrix, which is essential for homogeneity in material properties. The results show that the WEDM leads to localized melting along with material removal, specifically for both PAS reinforcement and aluminum matrix. Based on the microstructural characterization of the machined surface of WEDM-machined PAS-reinforced AA1050 composite, the surface morphology and machinability were mainly affected by the particle distribution, thermal impact, and crater formation. Thus, the results can lay a foundation for optimizing the parameters of WEDM for better surface integrity and machining efficiency.

3.2. Surface Roughness

Figure 7 presents a detailed surface texture analysis of the processed PAS-reinforced AA1050 composite. The 2D surface profile (Figure 7a) shows the topography of the machined surface, indicating particular surface features like the crater, which are generated owing to the rapid heating and cooling cycle involved in the WEDM process. The blue regions represent depressed landscape features (such as craters), and the red and yellow areas represent raised surface features. The 3D representation (Figure 7b) presents a volumetric view of the machined surface well, revealing the dimensionality of the craters and unevenness in spatial distribution. The crater types found at both the 2D and 3D sections suggest thermal erosion, dielectric flushing, and melting of the material during the WEDM process. The surface profile curve extracted (Figure 7c) illustrates the surface profile along a selected machining direction in grayscale levels. The results suggest microstructural inhomogeneity and thermal effect induced by WEDM discharge energy. The peaks and valleys of the profile hint at craters, melted areas, and layers of redeposited material. The formation of numerous craters and other irregular surface patterns demonstrates that WEDM processing significantly alters the surface morphology of PAS-reinforced AA1050. A 3D profile analysis highlights deep craters that may affect mechanical features, including wear resistance and fatigue life. Optimizing machining parameters is significant to achieve a better surface finish and enhanced material performance.

During the discharge phase, some material does not melt completely; instead, it solidifies into a layer known as “recast” after quenching in dielectric fluid. Based on careful examination, we find that surface roughness values vary from 2.1 µm to 3.55 µm, which is directly related to the rise in voltage. During the stir casting process, some of the PAS are

agglomerated, and they are not melted. Those PAS particles that are not melted contribute to roughness and crater formation observed in SEM.

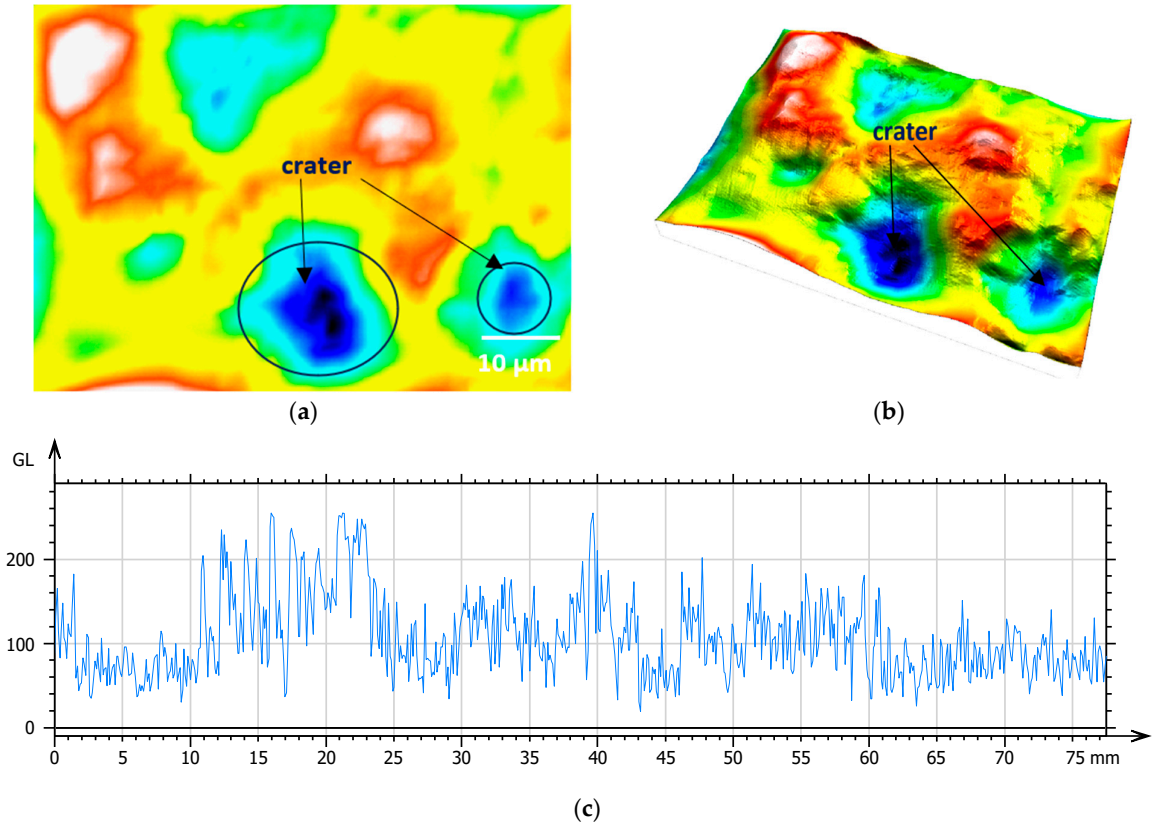


Figure 7. Surface texture analysis: (**a**) 2D profile, (**b**) 3D profile, and (**c**) Extracted individual profile.

3.3. Prediction of Material Removal Rate by Decision Tree Approach

Machine learning technique is used for predicting the optimum value for the relation between input and output variables [36]. The prediction of MRR is essential for optimizing machining processes. Recently, decision tree approaches have become more well-known in such prediction, because of their capacity to handle complex relationships between input and output variables. These machine learning algorithms utilize a tree-like structure to model decisions and their possible outcomes, making them highly effective for predicting MRR [37–39]. They can handle both categorical and continuous input variables, as well as nonlinear relationships between inputs and outputs. To predict MRR, input variables like voltage, current, and on/off pulses for the zinc-coated brass wire electrode to adjust cutting speed, as well as feed rate of the specimen material, are combined with output variables like MRR, surface roughness, and tool wear to form a data set. The data set is separated into two sets: the training set and the test set. The training set is used to train the decision tree model. Random forest prediction method employs a decision tree to model the correlation between input and output variables. The algorithm randomly selects a subset of features and builds multiple decision trees using them. Each decision tree makes independent predictions of the output variable, and the average of the individual tree predictions gives the final prediction. After training, the decision tree and random forest models were framed up to predict the MRR for new input data. By contrasting the actual MRR values from the test set with the anticipated predicted MRR values, the model's accuracy is evaluated. Parameters like the tree's maximum depth and the bare minimum of samples needed to divide a node can be changed to further improve the decision tree model's performance.

3.3.1. Data Visualization

Figure 8 shows the data visualization plot of MRR, electrode wear rate, SFR, and with respect to the applied voltage and various values of current for the combined experimental data of zinc-coated brass wire electrode. The observations were made with different current rates of 0.5 Amps, 1.0 Amps, and 1.5 Amps. Figure 8a demonstrates the connection between applied voltage and MRR, for the chosen current values, while Figure 8b shows the surface roughness data. Furthermore, Figure 8c depicts the electrode wear rate with respect to the applied voltage for a range of current choices. Subsequently, by considering the pulse ON periods of 1 µs, 2 µs, and 4 µs, the visualization of the electrode wear and MRR, SFR rate for the combined experimental data of zinc-coated brass wire electrode with respect to the applied voltage is shown in Figure 8.

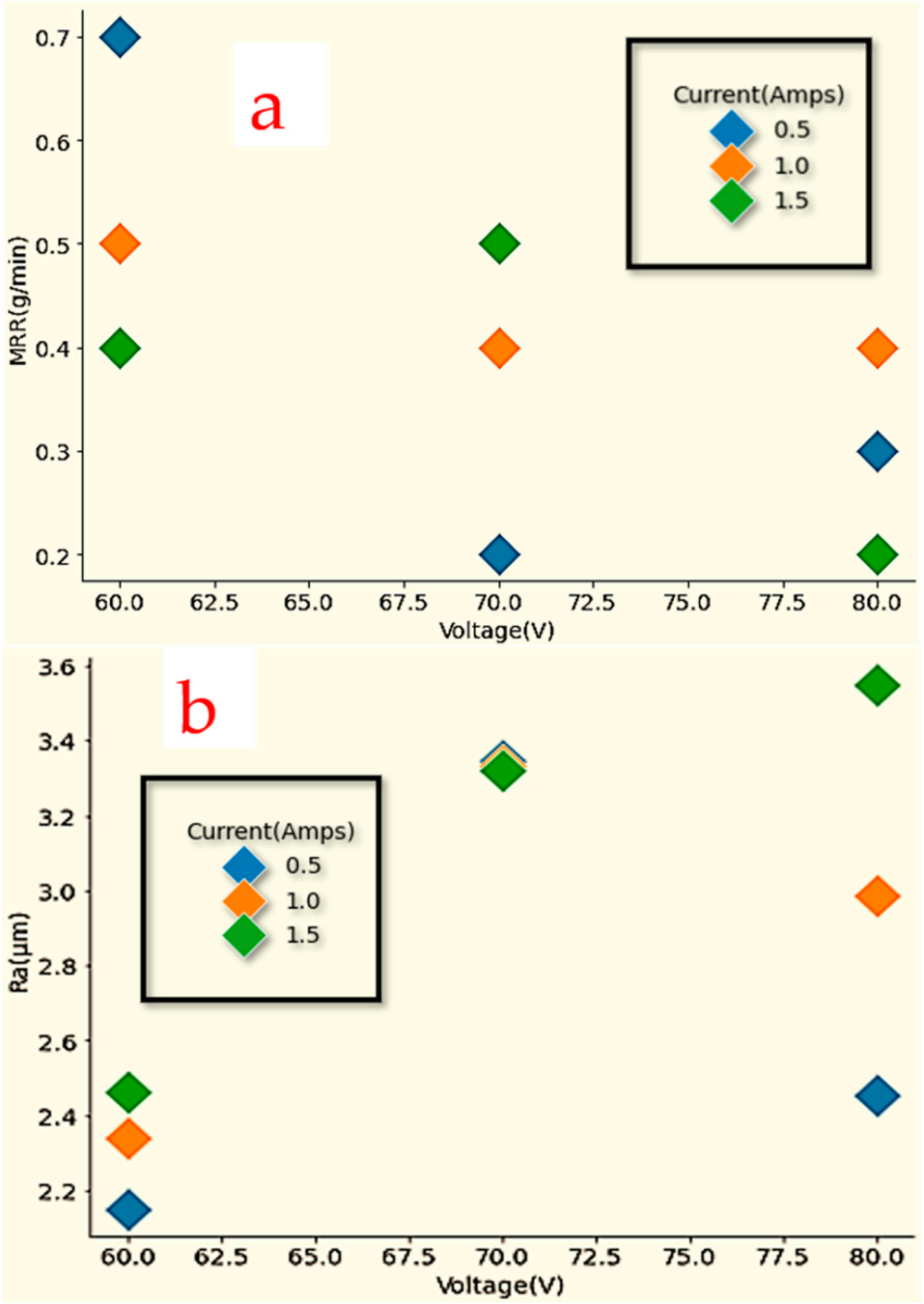


Figure 8. *Cont.*

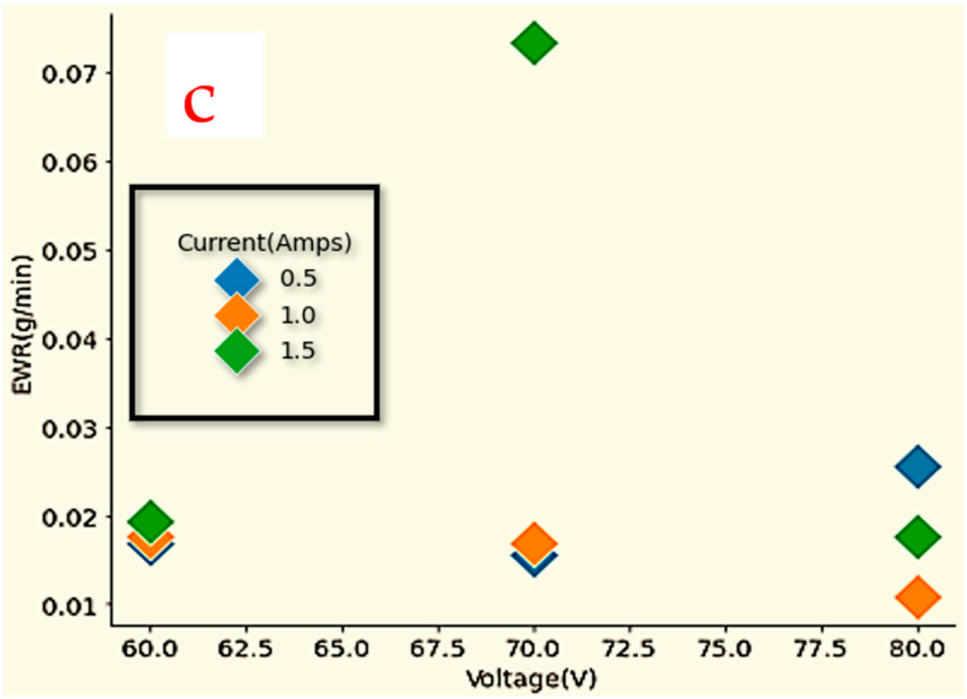


Figure 8. Data Visualization (**a**), material removal rate (**b**), surface roughness and (**c**) electrode wear rate.

In the illustration, Figure 9a shows the connection between the applied voltage and the MRR based on various pulse ON periods, while Figure 9b shows the surface roughness data. Additionally, Figure 9c depicts the electrode wear rate with respect to the applied voltage based on various pulse ON periods.

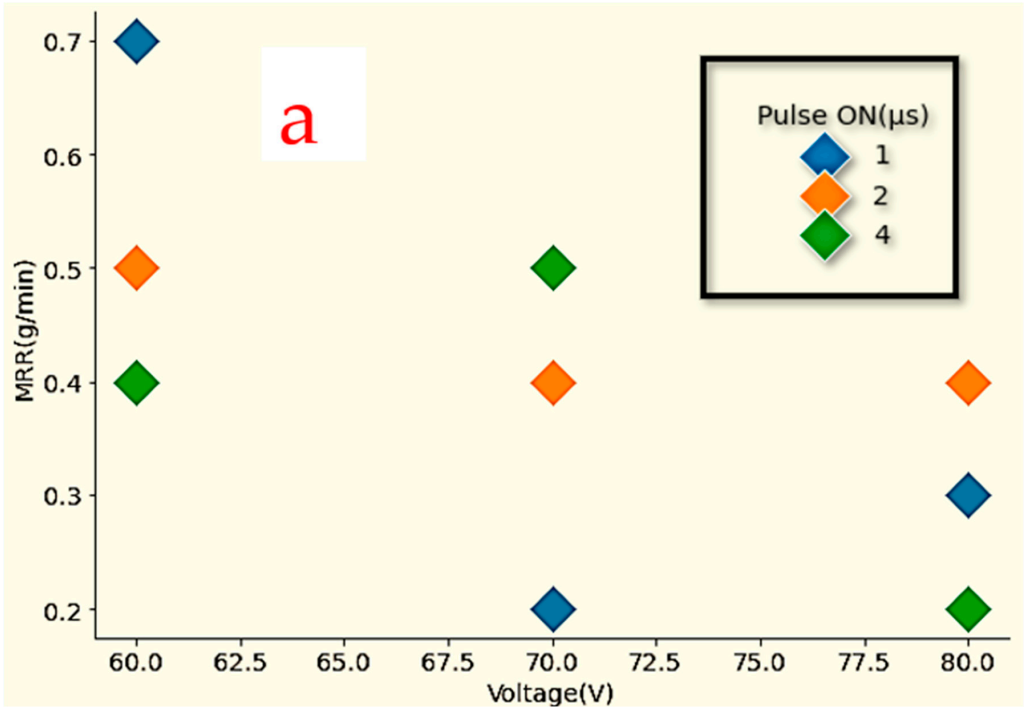


Figure 9. *Cont.*

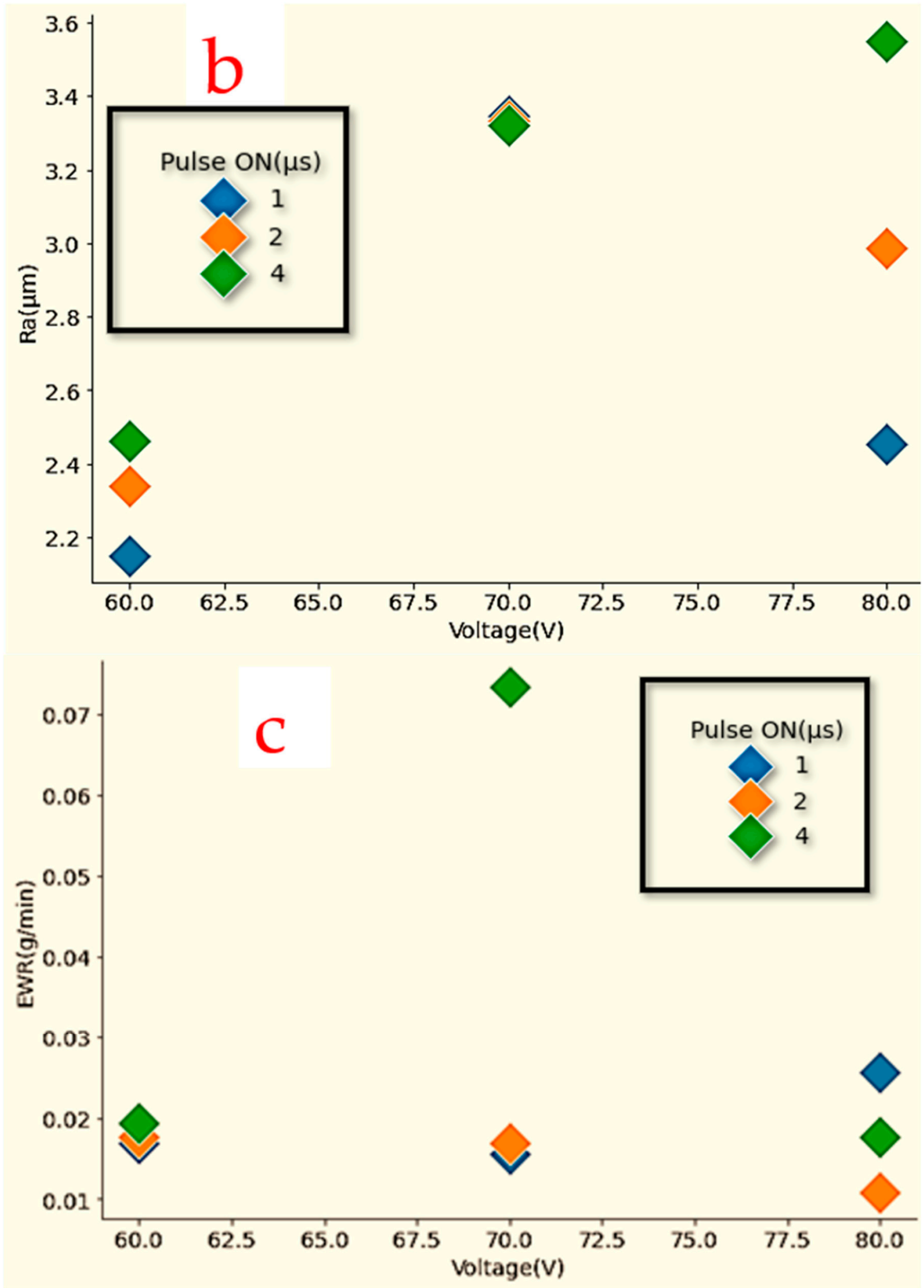


Figure 9. Data visualization of MRR (**a**), SFR (**b**), and EWR (**c**) in relation to the pulse ON duration and applied voltage for combined experimental data of zinc-coated brass wire electrode.

Figure 10 depicts a tree representation of the random forest prediction method for the MRR using the input current as the base parameter for the zinc-coated brass wire electrode. The figure shows the different decision trees in the random forest and their corresponding prediction paths, based on the status of pulses and voltage inputs. It is evident from the observation that the MRR is higher by 0.5 for the current above 0.750 Amps and the pulse on period of less than or equal to 3. From the subsequent observation made by using the input voltage as the base parameter.

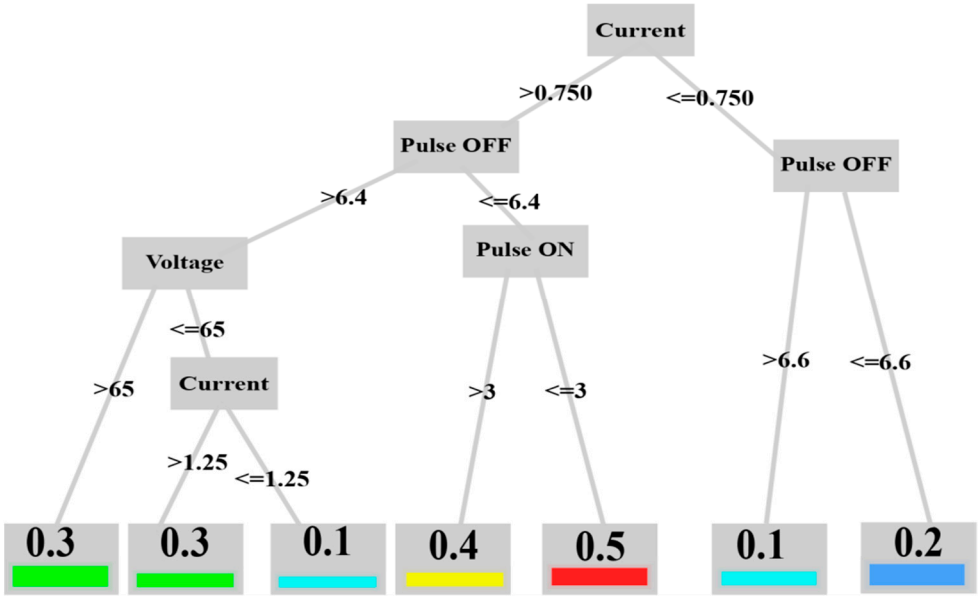


Figure 10. Tree representation of the random forest prediction of MRR under varying pulse conditions.

The random forest prediction outcomes for the MRR for the zinc-coated brass wire electrode. Figure 11 displays the various decision trees in the random forest and their prediction paths, indicating the role of the input voltage in predicting MRR. A better removal rate of 0.5 is observed for the voltage choices less than or equal to 65 volts, with the current choice of less than or equal to 0.75 Amps.

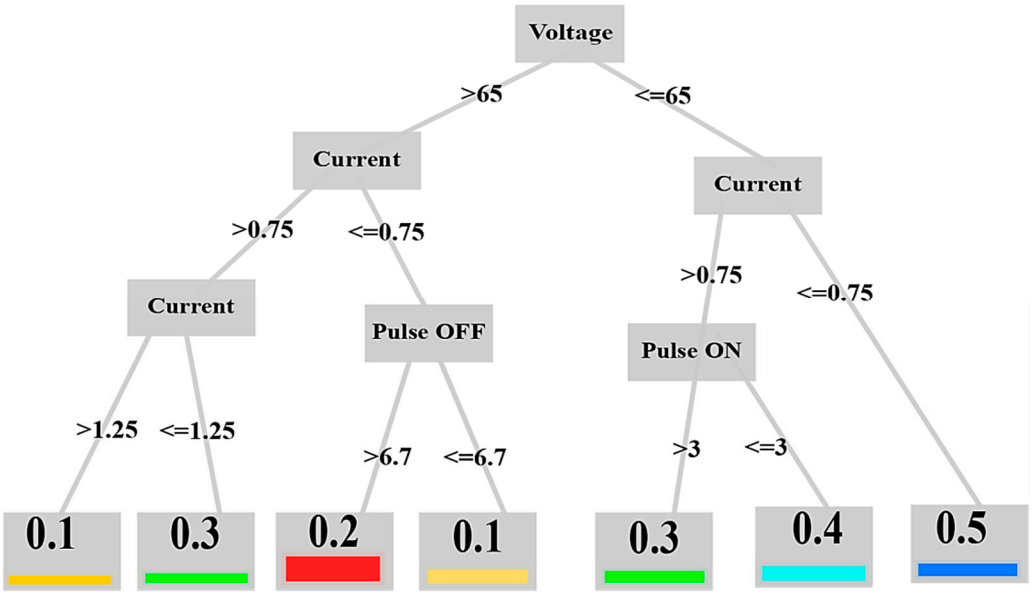


Figure 11. Decision tree representation showing the influence of voltage and current parameters on MRR.

3.3.2. Performance Evaluation of the Models

The decision tree approach uses Rapid Miner (Ver. 9.2) software, which integrates all information needed to make decisions. To effectively train the model, the original 18 data sets were replicated five times, resulting in 90 data points being input into the software. The decision tree model was evaluated using classification statistics like F1 scores, recall, and precision. The model's F1-score was 0.94, its precision was 0.92, and its recall was 0.96. The random forest model, which uses an ensemble learning technique, achieved a

0.94 F1-score, 0.97 precision, and 0.96 recall. The mentioned experimental and analytical study employs selected features from decision trees and random forest prediction methods to frame regression models for examining the MRR in relation to the electrodes made of zinc.

4. Conclusions

AA 1050 reinforced with 3% wt. snail shell was machined by wire cut electro discharge machining using zinc-coated brass wire electrode, varying the process conditions. The addition of Snail Shell reinforcement increased the hardness of the composite, which consequently affected its machining performance. SEM images show that the work surface had microvoids, a few macrovoids, intergranular cracks, and shallow craters. The random forest approach achieved a precision of 0.97, a recall of 0.96, and an F1-score of 0.94, whereas the decision tree model obtained a precision of 0.92, a recall of 0.96, and an F1-score of 0.94. A high material removal rate of 0.5 mm^3/min was observed for the voltage choices less than or equal to 65 volts with the current choice of less than or equal to 0.75 Amps, resulting in 2.14 μm surface roughness and 0.017 electrode wear ratio. PAS particle size is expected to significantly influence MRR and SR, and investigating this effect is planned for future work. While cross-validation was performed on the available data, the use of a dedicated, independent test set was not feasible due to the limited dataset size, which is planned for future work.

The industrial implications of this research are broad and impactful, representing a massive step forward in manufacturing processes within multiple key sectors. Using the optimized machining process to facilitate superior utilization of bio-ceramic reinforced AA1050 composites results in an improvement in performance characteristics, which consequently makes such beneficial interventions more durable and sustainable. This research could drive advancements in many sectors by satisfying the needs of those industries with lightweight, high-strength, and engineered-to-precision component production, paving the way for advanced design and manufacturing technologies for diverse sectors as well. This high level of machining outcome control enables the manufacture of complex, individualized parts that meet specific performance demands—like personalized medical implants or aerospace and automotive components.

The current study focuses more on machining parameter optimization and performance characteristics for bio-ceramic reinforced AA1050 composite. Nevertheless, we are well aware of the significance of sustainability aspects and acknowledge that these are fundamental criteria for a more widespread implementation as well as durability in the long run when it comes to implementing such materials and processes on an industrial scale. Given these limitations, future work is to examine sustainability by checking machining energy efficiency and performing a life-cycle assessment (LCA) for the environmental impact of utilizing waste snail shells as reinforcement. This will involve an investigation of WEDM's energy use and the assessment of the benefits and drawbacks for the environment connected to recycling natural waste snail shells.

Author Contributions: Conceptualization, R.J.H.N.; methodology, R.J.H.N. and D.S.S.P.K.; formal analysis, S.K.J.; investigation, R.J.H.N. and A.J.S.J.; writing—original draft preparation, R.J.H.N. and D.S.S.P.K.; writing—review and editing, A.J.S.J.; supervision, R.J.H.N. All authors have read and agreed to the published version of the manuscript.

Funding: This research received no external funding.

Data Availability Statement: The datasets presented in this article are not readily available due to technical and time limitations.

Conflicts of Interest: The authors declare no conflict of interest.

References

1. Hassanzadeh-Aghdam, M.K.; Haghgoo, M.; Ansari, R. Micromechanical study of elastic plastic and thermoelastic behaviors of SiC nanoparticle-reinforced aluminum nano composites. *Mech. Mater.* **2018**, *121*, 1–9. [CrossRef]
2. Hourmand, M.; Sarhan, A.A.; Farahany, S.; Sayuti, M. Microstructure characterization and maximization of the material removal rate in nano-powder mixed EDM of Al-Mg_2Si metal matrix composite—ANFIS and RSM approaches. *Int. J. Adv. Manuf. Technol.* **2019**, *101*, 2723–2737. [CrossRef]
3. Lu, T.; He, T.; Li, Z.; Chen, H.; Han, X.; Fu, Z.; Chen, W. Microstructure, mechanical properties and machinability of particulate reinforced Al matrix composites: A comparative study between SiC particles and high-entropy alloy particles. *J. Mark. Res.* **2020**, *9*, 13646–13660. [CrossRef]
4. Garg, P.; Jamwal, A.; Kumar, D.; Sadasivuni, K.K.; Hussain, C.M.; Gupta, P. Advance research progresses in aluminium matrix composites: Manufacturing & applications. *J. Mark. Res.* **2019**, *8*, 4924–4939.
5. Hynes, N.R.J.; Kumar, D.S.P.; Prabhu, M.V.; Ali, M.A.; Raza, M.H.; Pruncu, C.I. Investigating the parametric effects on wire electric discharge machining performance in processing AA1050-5 wt.% SiC composite with zinc-coated brass wire. *J. Braz. Soc. Mech. Sci. Eng.* **2022**, *44*, 127. [CrossRef]
6. Razavykia, A.; Farahany, S.; Yusof, N.M. Evaluation of cutting force and surface roughness in the dry turning of Al–Mg2Si in situ metal matrix composite inoculated with bismuth using DOE approach. *Measurement* **2015**, *76*, 170–182. [CrossRef]
7. Hynes, N.R.; Raja, S.; Tharmaraj, R.; Pruncu, C.I.; Dispinar, D. Mechanical and tribological characteristics of boron carbide reinforcement of AA6061 matrix composite. J Braz. *Soc. Mech. Sci. Eng.* **2020**, *42*, 155. [CrossRef]
8. Farooq, M.U.; Ali, M.A.; He, Y.; Khan, A.M.; Pruncu, C.I.; Kashif, M.; Ahmed, N.; Asif, N. Curved profiles machining of Ti6Al4V alloy through WEDM: Investigations on geometrical errors. *J. Mater. Res. Technol.* **2020**, *9*, 16186. [CrossRef]
9. Manikandan, K.; Palanikumar, K. Machinability evaluation and comparison of Incoloy 825, Inconel 603 XL, Monel K400 and Inconel 600 super alloys in wire electrical discharge machining. *J. Mark. Res.* **2020**, *9*, 12260–12272. [CrossRef]
10. Mouralova, K.; Kovar, J.; Klakurkova, L.; Bednar, J.; Benes, L.; Zahradnicek, R. Analysis of surface morphology and topography of pure aluminium machined using WEDM. *Measurement* **2018**, *114*, 169–176. [CrossRef]
11. Shayan, A.V.; Afza, R.A.; Teimouri, R. Parametric study along with selection of optimal solutions in dry wire cut machining of cemented tungsten carbide (WC-Co). *J. Manuf. Process* **2013**, *15*, 644–658. [CrossRef]
12. Chaubey, S.K.; Jain, N.K. Investigations on surface quality of WEDM-manufactured meso bevel and helical gears. *Mater. Manuf. Process.* **2018**, *33*, 1568–1577. [CrossRef]
13. Mandaloi, G.; Singh, S.; Kumar, P.; Pal, K. Efect on crystalline structure of AISI M2 steel using tungsten–thorium electrode through MRR, EWR, and surface fnish. *Measurement* **2016**, *90*, 74–84. [CrossRef]
14. Manna, A.; Kumar, R. Modeling and desirability approach-based multi-response optimization of WEDM parameters in machining of aluminum metal matrix composite. *J. Braz. Soc. Mech. Sci. Eng.* **2018**, *40*, 458.
15. Ishfaq, K.; Anwar, S.; Ali, M.A.; Raza, M.H.; Farooq, M.U.; Ahmad, S.; Pruncu, C.I.; Saleh, M.; Salah, B. Optimization of WEDM for precise machining of novel developed Al6061–7.5% SiC squeeze-casted composite. *Int. J. Adv. Manuf. Technol.* **2020**, *111*, 2031–2049. [CrossRef]
16. Pramanik, A.; Littlefair, G. Wire EDM mechanism of MMCs with the variation of reinforced particle size. *Mater. Manuf. Process.* **2016**, *31*, 1700–1708. [CrossRef]
17. Gopal, P.M.; Prakash, K.S.; Jayaraj, S. WEDM of Mg/CRT/BN composites: Effect of materials and machining parameters. *Mater. Manuf. Process* **2018**, *33*, 77–84. [CrossRef]
18. Suresh, S.; Sudhakara, D. Investigations on wire electric discharge machining and mechanical behavior of Al 7075/nano-SiC composites. *J. Inst. Eng. Ser. D* **2019**, *100*, 217–227. [CrossRef]
19. Kumar, S.S.; Uthayakumar, M.; Kumaran, S.T.; Parameswaran, P.; Mohandas, E.; Kempulraj, G.; Babu, B.R.; Natarajan, S.A. Parametric optimization of wire electrical discharge machining on aluminium based composites through grey relational analysis. *J. Manuf. Process* **2015**, *20*, 33–39. [CrossRef]
20. Karthik Pandiyan, G.; Prabaharan, T.; Jafrey Daniel James, D.; Sivalingam, V.; Thangapandian, N. Improvement on the machinability characteristics of AA6061-T6/15 wt.% SiC composites by response surface methodology. *Surf. Topogr. Metrol. Prop.* **2021**, *9*, 035050.
21. Lal, S.; Kumar, S.; Khan, Z.A.; Siddiquee, A.N. Wire electrical discharge machining of AA7075/ SiC/Al_2O_3 hybrid composite fabricated by inert gas-assisted electromagnetic stir-casting process. *J. Braz. Soc. Mech. Sci. Eng.* **2014**, *36*, 335–346. [CrossRef]
22. Dey, A.; Pandey, K.M. Selection of optimal processing condition during WEDM of compo casted AA6061/cenosphere AMCs based on grey-based hybrid approach. *Mater. Manuf. Process.* **2018**, *33*, 1549–1558. [CrossRef]
23. Raza, M.H.; Wasim, A.; Ali, M.A.; Hussain, S.; Jahanzaib, M. Investigating the effects of different electrodes on Al6061-SiC-7.5 wt% during electric discharge machining. *Int. J. Adv. Manuf. Technol.* **2018**, *99*, 3017–3034. [CrossRef]
24. Reolon, L.W.; Henning Laurindo, C.A.; Torres, R.D.; Amorim, F.L. WEDM performance and surface integrity of Inconel alloy IN718 with coated and uncoated wires. *Int. J. Adv. Manuf. Technol.* **2019**, *100*, 1981–1991. [CrossRef]

25. Manjaiah, M.; Narendranath, S.; Basavarajappa, S.; Gaitonde, V.N. Efect of electrode material in wire electro discharge machining characteristics of Ti50Ni50−xCux shape memory alloy. *Precis. Eng.* **2015**, *41*, 68–77. [CrossRef]
26. Nourbakhsh, F.; Rajurkar, K.P.; Malshe, A.P.; Cao, J. Wire electro-discharge machining of titanium alloy. *Procedia CIRP* **2013**, *5*, 13–18. [CrossRef]
27. Ramamurthy, A.; Sivaramakrishnan, R.; Muthuramalingam, T.; Venugopal, S. Performance analysis of wire electrodes on machining Ti-6Al-4V alloy using electrical discharge machining process. *Mach. Sci. Technol.* **2015**, *19*, 577–592. [CrossRef]
28. Shandilya, P.; Jain, P.K.; Jain, N.K. RSM and ANN modeling approaches for predicting average cutting speed during WEDM of SiC/6061 Al MMC. *Proc. Eng.* **2013**, *64*, 767–774. [CrossRef]
29. Rao, T.B.; Krishna, A.G. Selection of optimal process parameters in WEDM while machining Al7075/SiC metal matrix composites. *Int. J. Adv. Manuf. Technol.* **2014**, *73*, 299–314. [CrossRef]
30. Raju, S.S.; Rao, G.S.; Samantra, C. Wear behavioral assessment of Al-CSAp-MMCs using grey-fuzzy approach. *Measurement* **2019**, *140*, 254–268. [CrossRef]
31. Udaya Prakash, J.; Ananth, S.; Jebarose Juliyana, S.; John Paul, P. *Efect of Wire EDM Process Parameters on Machining of Aluminium Matrix Composites (356/Fly Ash)*; Springer: Singapore, 2020.
32. Pruncu, C.I.; Vladescu, A.; Hynes, N.R.J.; Sankaranarayanan, R. Surface Investigation of Physella Acuta Snail Shell Particle Reinforced Aluminium Matrix Composites. *Coatings* **2022**, *12*, 794. [CrossRef]
33. Hynes, N.R.J.; Sankaranarayanan, R.; Sujana, J.A.J.; Krolczyk, G.M.; Ene, A. Decision tree approach based green flow drilling of hybrid aluminium matrix composites using eco-friendly coolants. *J. Manuf. Process.* **2022**, *80*, 178–186. [CrossRef]
34. Sen, R.; Choudhuri, B.; Barma, J.D.; Chakraborti, P. An investigation on the effect of different coated electrodes on the surface quality of WEDM by varying discharge energy level. *Int. J. Adv. Manuf. Technol.* **2020**, *106*, 3285–3299. [CrossRef]
35. Kapoor, J.; Singh, S.; Khamba, J.S. High-performance wire electrodes for wire electrical-discharge machining—A review. *Proc. Inst. Mech. Eng. Part B J. Eng. Manuf.* **2012**, *226*, 1757–1773. [CrossRef]
36. Kapoor, J.; Singh, S.; Khamba, J.S. Recent developments in wire electrodes for high performance WEDM. In Proceedings of the World Congress on Engineering, London, UK, 30 June–2 July 2010.
37. Sankaranarayanan, R.; Hynes, N.R.J.; Kumar, J.S.; Sujana, J.A.J. Random decision forest based sustainable green machining using Citrullus lanatus extract as bio-cutting fluid. *J. Manuf. Process.* **2021**, *68 Pt A*, 1814–1823. [CrossRef]
38. Hynes, N.R.J.; Sankaranarayanan, R.; Sujana, J.A.J. A decision tree approach for energy efficient friction riveting of polymer/metal multi-material lightweight structures. *J. Clean. Prod.* **2021**, *292*, 125317. [CrossRef]
39. Sankaranarayanan, R.; Navasingh, R.J.H.; Sujana, A.J.; Čep, R. Bio-coolants for sustainable friction drilling process: A machine learning approach to temperature reduction. *Results Eng.* **2025**, *26*, 104959. [CrossRef]

Disclaimer/Publisher's Note: The statements, opinions and data contained in all publications are solely those of the individual author(s) and contributor(s) and not of MDPI and/or the editor(s). MDPI and/or the editor(s) disclaim responsibility for any injury to people or property resulting from any ideas, methods, instructions or products referred to in the content.